Magnetic bistability in a submonolayer of sublimated Fe_4 Single-Molecule Magnets

Luigi Malavolti,[†] Valeria Lanzilotto,[†] Silviya Ninova,[†] Lorenzo Poggini,[†] Irene Cimatti,[†]

Brunetto Cortigiani,[†] Ludovica Margheriti,[†] Daniele Chiappe,[‡] Edwige Otero,[§]

Philippe Sainctavit,[§,£]

Federico Totti,[†] Andrea Cornia,[$] Matteo Mannini,[†] and Roberta Sessoli[†]*

[†]Department of Chemistry 'Ugo Schiff' and INSTM Research Unit, University of Florence, 50019 Sesto Fiorentino, Italy

[‡]Department of Physics, University of Genova, 16146 Genova, Italy

[§]Synchrotron SOLEIL, L'Orme des Merisiers, Saint Aubin BP48 91192 Gif-sur-Yvette Cedex, France

[£]IMPMC, UMR7590 CNRS, Université Pierre et Marie Curie, MNHN, IRD, 75005 Paris, France

[$]Department of Chemical and Geological Sciences and INSTM Research Unit, University of Modena and Reggio Emilia, 41125 Modena, Italy

KEYWORDS: Single molecule magnet, scanning tunneling microscopy, X-ray magnetic circular dichroism, density functional theory.

ABSTRACT

We demonstrate that Fe_4 molecules can be deposited on gold by thermal sublimation in ultra-high vacuum with retention of single molecule magnet behavior. A magnetic hysteresis comparable to that found in bulk samples is indeed observed when a submonolayer film is studied by X-ray magnetic circular dichroism. Scanning tunneling microscopy evidences the coexistence of Fe_4 molecules assembled in a 2D lattice with short-range hexagonal order and traces of a smaller contaminant. The presence of intact Fe_4 molecules and the retention of their bistable magnetic behavior on the gold surface evidenced by our low temperature synchrotron characterization are supported by density functional theory calculations.

Molecules exhibiting magnetic hysteresis, also known as Single Molecule Magnets (SMMs), have been the target of intense research as they represent the ultimate miniaturization limit of magnetic memories, with a profusion of quantum effects governing the dynamics of the magnetization.[1–4] Recent efforts have focused on the investigation of individual SMMs by either depositing them on a conducting surface and using the lateral resolution of scanning probe techniques[5–7] or inserting them in nanojunctions and nanostructures.[8–13] The most investigated system is bis(phthalocyaninato)terbium(III) ($TbPc_2$), a neutral complex characterized by a huge anisotropy barrier for the reversal of the magnetization and a remarkable chemical stability.[14] In the bulk phase, it exhibits a moderately high-temperature hysteresis that was found to persist when deposited on highly oriented pyrolitic graphite[15,16] or chemisorbed on a silicon surface.[17] However, magnetic bistability disappears upon sublimation on metallic surfaces.[18–22] Earlier reports focused also on tetrairon(III) (Fe_4) clusters with a propeller-like structure, which display a much weaker anisotropy and sub-kelvin blocking temperatures. Significantly, sulfur-

functionalized complexes of this class retain a molecular hysteresis once chemisorbed as monolayers (MLs) on a gold substrate.[23,24] Specific Fe_4 derivatives were also found to withstand thermal sublimation; with this procedure, thick films were deposited on a non-conductive substrate and shown to retain slow relaxation of the magnetization.[25,26] To the best of our knowledge, no magnetic or morphologic characterizations of Fe_4 ultrathin films sublimated on a conductive substrate have been reported yet. Such a statement can be also extended to computational studies on Fe_4 clusters adsorbed on surfaces.

In this work we have exploited the robustness of Fe_4 SMMs to grow submonolayer films on gold substrates by thermal sublimation. The adsorption of these complex molecules on Au(111) single crystal has been studied by means of scanning tunneling microscopy (STM) in ultra-high-vacuum conditions (UHV). Very low-temperature X-ray Magnetic Circular Dichroism (XMCD) experiments have provided direct access to magnetic behavior, confirming the retention of SMM properties also at submonolayer coverage. These cutting-edge experimental efforts have been flanked by state-of-art structural and magnetic Density Functional Theory (DFT) analysis. Overall, a sound and in-depth picture of the adsorption process as well as of the electronic and magnetic properties of Fe_4 SMMs on gold emerged clearly from the study here presented. The results prove that fully-functional SMMs can be organized in a submonolayer in vacuum conditions, an achievement of relevance for molecular spintronics.

The specific derivative herein considered is $[Fe_4(L)_2(dpm)_6]$ (**Fe_4Ph**), where H*dpm* is dipivaloylmethane and H_3L is the tripodal ligand 2-hydroxymethyl-2-phenylpropane-1,3-diol. The Fe^{III} ions (s = 5/2, high spin) adopt a metal centered triangular topology in the structure, as shown in Fig. 1a. Two tripodal ligands, one above and one below the plane of the four Fe^{III} ions, act as bridges and promote an antiferromagnetic interaction between the central spin and the

peripheral ones. A ground state with total spin S = 5, schematized by the arrows in Fig. 1a, is selectively populated at liquid helium temperature. This family of SMMs is characterized by a moderate uniaxial magnetic anisotropy along the normal (z) to the plane defined by the four metal ions, described in first approximation by the spin Hamiltonian $H_{an} = DS_z^2$; here, S_z is the z-component of the total spin operator for the ground state and $\frac{D}{k_b} \approx -0.6$ K. The potential barrier to be overcome in order to invert the magnetization, given in first approximation by $\Delta E = DS^2$, is thus only 15 K while a hysteresis loop opens only slightly below 1 K.

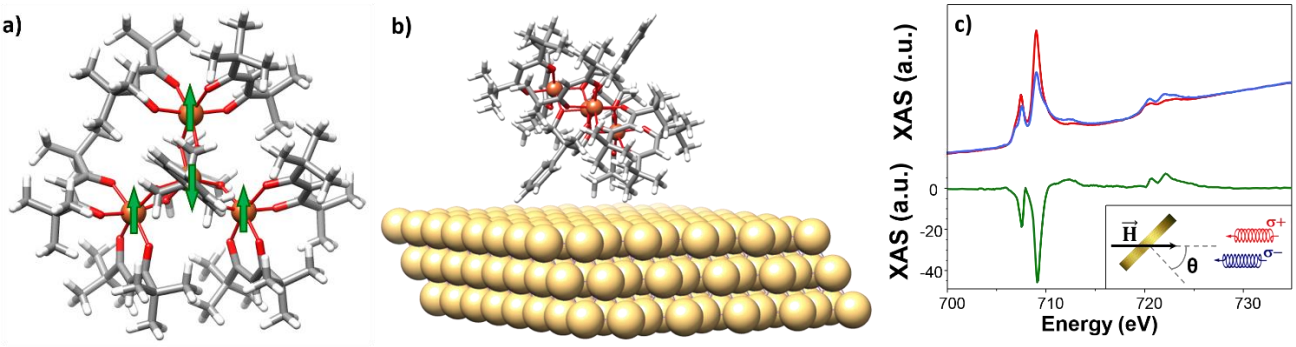

Figure 1: (a) **Fe$_4$Ph** molecular structure viewed along the idealized C_3 axis, with arrows depicting the ferromagnetic arrangement of the Fe^{III} spins in the ground S = 5 state; color code: Fe = orange, O = red, C = grey, H = light grey. (b) DFT optimized geometry of the **Fe$_4$Ph** molecules deposited on Au substrate, showing that the idealized C_3 axis forms an angle of ca. 35° with the normal to the surface. (c) X-ray absorption spectra at the Fe $L_{2,3}$ edges acquired at 0.68 K with 30 kOe field and θ = 0°, where σ^+ and σ^- are the red and blue curves, respectively; the derived XMCD% spectrum is shown in green (see Supporting Information (SI) for details). The scheme reported in the inset of panel (c) shows the setup geometry adopted during the XMCD experiments.

The synthesis of **Fe$_4$Ph**·Et$_2$O and the characterization of thermally sublimated thick films were reported earlier.[25] A temperature window ranging from 480 to 570 K, depending on experimental conditions, was individuated for the thermal evaporation of intact molecules in high vacuum.[25,26] TGA analysis in N_2 flux indicates that loss of Et$_2$O takes place gradually below 480 K and that the desolvated solid is stable up at least 540 K. In the present study large single crystals of **Fe$_4$Ph**·Et$_2$O were crushed and employed as high purity starting material for deposition of submonolayer films by using a home-made Knudsen cell. Coverage estimation was made by comparing XPS and XAS data with those acquired for a chemisorbed layer of a thioacetyl-substituted Fe$_4$ SMM on gold which was taken as the monolayer reference (see Supporting Information, SI). As for the XMCD measurements, we referred to XAS signal recorded at the Fe L_3 edge, while for the *in-house* STM investigation the XPS Fe *2p* / Au *4f* intensity ratio was used. Moreover, the XPS-based coverage evaluation was further confirmed by STM experiments. Two coverages, corresponding to 0.2 and 0.8 ML, were then selected for the *in-situ* STM characterization. In order to reduce the mobility of the molecules on the surface and improve lateral resolution, the images were acquired by cooling the sample to 30 K; furthermore, a low tunneling current, *i.e.* below 10 pA, was employed in order to prevent damaging of the Fe$_4$ molecules. The STM images for the 0.2 ML sample are shown in Fig. 2a,b. The **Fe$_4$Ph** molecules appear to form densely packed islands of approximately spherical objects with average lateral dimensions of *ca.* 1.66 ± 0.20 nm (Fig. 2c), which are comparable to those expected for intact **Fe$_4$Ph** (*ca.* 1.8 nm for the largest dimension)[27] based on the optimized structure by DFT calculation (see below and Fig. 2e).

Along with spherical objects, the sample shows domains with rather different appearance whose internal structure could not be resolved (Fig. S2.1). Their height (0.30 ± 0.05 nm), though

determined by STM and therefore convoluted with density of states, suggests that they cannot be associated with **Fe_4Ph** molecules but rather with smaller units, either contaminants or fragments. We notice that before deposition the pristine material was subject to a long degasing process (several hours at 473 K) in order to eliminate volatile contaminants, such as Et_2O or traces of free ligands. On the other hand, the sublimation and thermal decomposition temperatures of **Fe_4Ph** (488 K and *ca.* 508 K, respectively) are close to each other, so that a partial decomposition of the **Fe_4Ph** molecule during the sublimation process cannot be ruled out. As an alternative explanation, an on-surface decomposition process may occur, involving reactive sites on the Au(111) substrate.

The contaminant seems to have a high sticking coefficient on the bare gold substrate covering a significant part of it (see Fig. 2a). This result has obvious consequences on the adsorption process of the **Fe_4Ph** molecules. Indeed, the **Fe_4Ph** islands show a broad and asymmetric heights distribution with two different contributions centered at 0.82 ± 0.11 nm and 1.05 ± 0.11 nm, respectively. The difference between the two centers is comparable to the height of the aforementioned contaminant domains, suggesting that a fraction of the **Fe_4Ph** molecules are directly in contact with the gold substrate, while the remaining molecules lie on the contaminants.

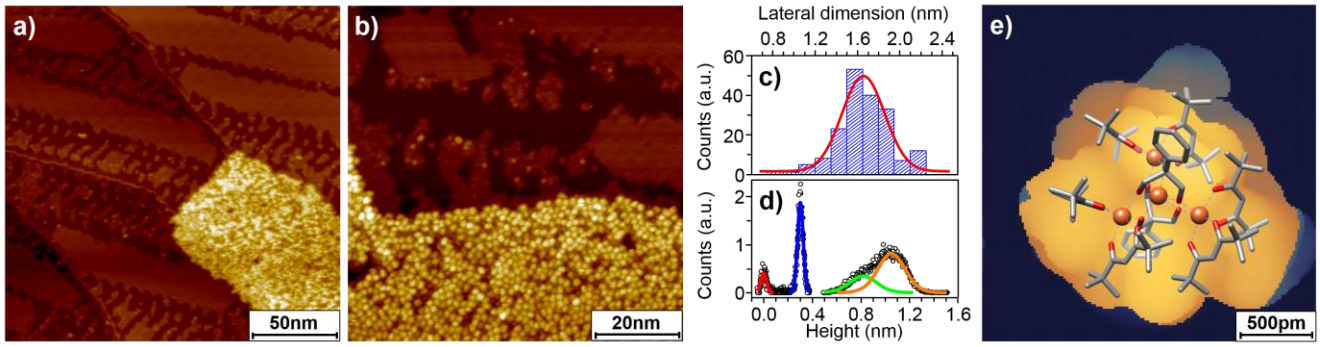

Figure 2. STM images acquired at 30 K for **Fe$_4$Ph** sublimated on Au(111) single crystal. (a) Large scale image of the 0.2 ML sample (135×135 nm^2, 3 pA, 2.5 V). (b) Same sample investigated at higher magnification (80×80 nm^2, 10 pA, 2.0 V). (c) Lateral size distribution of the **Fe$_4$Ph** molecules extracted from image (b) along with its Gaussian fit. (d) Height distributions in (b) with the red Gaussian reproducing the roughness of the bare gold while the blue one reproduces the height distribution of the contaminants domains; two Gaussian curves are used to reproduce the broad height distribution associated to the **Fe$_4$Ph** molecules (green and orange lines). (e) Calculated STM image of **Fe$_4$Ph** adsorbed on Au(111) at 2 V bias (occupied states), superimposed on the DFT-optimized structure.

Increasing the coverage to *ca.* 0.8 ML a slightly different situation is observed. The large scale image (Fig. 3a) shows the presence of a homogeneous first layer which is characterized by the presence of few second-layer islands and meandering hollows. Within the first layer, the molecules tend to spread forming an almost complete single layer suggesting a *quasi* layer-by-layer growth of the molecular film. As shown in Fig. 3b the molecules of dimension 1.63 ± 0.24 nm (Fig. 3c) are organized in densely packed domains with short range hexagonal order. At this coverage the contaminants domain cannot be identified. It is interesting to notice that a unique height distribution is detected, centered at 0.82 ± 0.12 nm (see Fig.3d), thus practically identical to one of the two contributions observed for the 0.2 ML coverage. A similar height is estimated for the second layer (0.96 ± 0.13 nm, see Fig. S2.2in SI). It is therefore impossible to assess if, for higher coverages, the **Fe$_4$Ph** molecules are deposited directly on gold or on a full monolayer of contaminants.

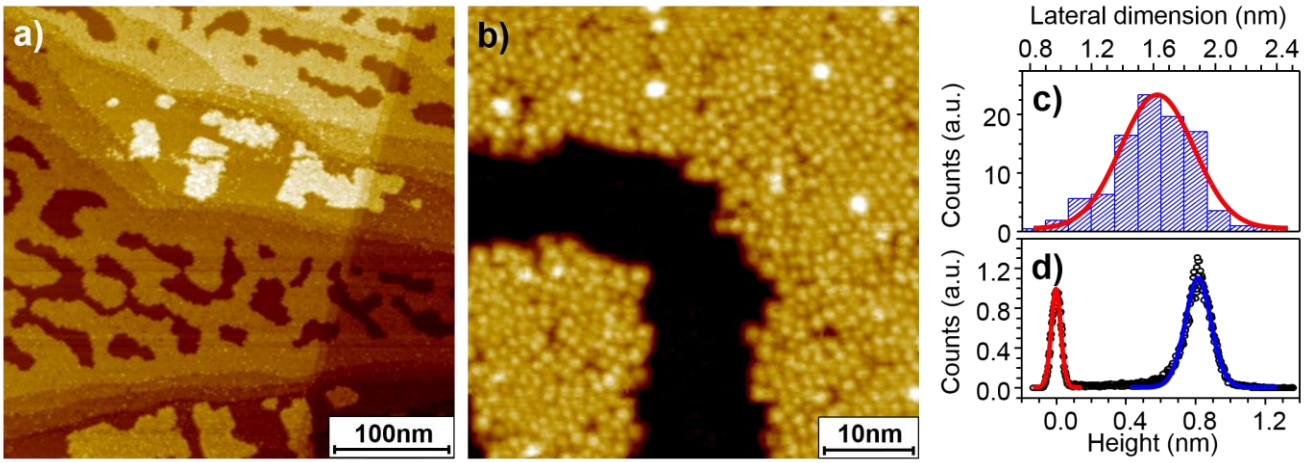

Figure 3. (a) STM image of the 0.8 ML sublimated sample of **Fe$_4$Ph** (389×389 nm^2, 10 pA, 2.0 V). (b) Enlarged view of the same surface (50×50 nm^2, 10 pA, 2.0 V). (c) Lateral size distribution of the **Fe$_4$Ph** molecules extracted from image (b) along with its Gaussian fit. (d) Height distributions in (b) with the red and blue Gaussian fits reproducing the roughness inside the hollows and the height distribution within the **Fe$_4$Ph** layer, respectively.

In order to get a deeper insight, the interaction of **Fe$_4$Ph** with the Au(111) surface was investigated by a periodic-DFT approach based on the revPBE functional[28] plus D3 dispersion corrections[29] (see SI for details). The optimized structure of **Fe$_4$Ph** adsorbed on the metal is reported in Fig 1b. The molecule revealed to be rigid enough to keep its core geometry almost unchanged, as it is evident from Fig. 1b, with changes which do not exceed one degree for the average Fe-O-Fe bridging angle (see Table S4.2). The easy axis of the magnetization, taken as the normal to the plane containing the four iron ions, was evaluated to form an angle of 34.4° with the normal to the surface. This value is close to the one found for a thioacetyl functionalized analogue, chemically grafted to the Au(111) surface.[24] We notice that the physisorption energy of **Fe$_4$Ph** (40.3 kcal mol^{-1}) is due mainly to the large number of favorable Au-H interactions,

whose contribution is however expected to be overestimated by the employed D3 energy dispersion corrections.[29]

On the basis of the DFT optimized structure it has been possible to simulate (Fig. 2e) an STM image of the **Fe$_4$Ph** molecule on Au(111). Due to the low conductivity of the ligands shell a quasi-spherical multi-lobed structure is visible in line with experiment, though the sub-molecular resolution is not as high as for flat molecules like $TbPc_2$. An average diameter of *ca.* 1.9 nm can be estimated from the computed image, in agreement with the experimental STM values.

As far as the magnetic properties of **Fe$_4$Ph** adsorbed on gold are concerned, the evaluation of its magnetic structure was performed using the well-established Broken Symmetry (BS) formalism[30,31] within the DFT framework and developing the approach reported in ref.[32] Such an approach allows to estimate the value of the exchange-coupling constants in the spin Hamiltonian written as:

$$H_{ex} = J_1(\boldsymbol{S_1}\cdot\boldsymbol{S_2} + \boldsymbol{S_1}\cdot\boldsymbol{S_3} + \boldsymbol{S_1}\cdot\boldsymbol{S_4}) + J_2(\boldsymbol{S_2}\cdot\boldsymbol{S_3} + \boldsymbol{S_3}\cdot\boldsymbol{S_4} + \boldsymbol{S_2}\cdot\boldsymbol{S_4}) \qquad \textbf{eq. 1}$$

where threefold symmetry is assumed and J_1 and J_2 account for nearest-neighbor and next-nearest neighbor interactions, respectively. A spin Hamiltonian with lower symmetry was also tested (see Table S4.1 and SI for more details) resulting however in negligible deviations from threefold symmetry.

It is well known that the inclusion of Hartree-Fock (HF) exchange by using hybrid functional is necessary to accurately evaluate magnetic interactions.[33] We applied this approach first, using the PBE0 functionals.[34] Table 1 shows that good agreement with the experimental *J* values is observed when the X-ray crystallographic structure or the optimized geometry of **Fe$_4$Ph** molecules are considered. When the molecules are adsorbed on gold, the approach based on

hybrid functionals is however computationally too demanding. The calculation was therefore performed on the optimized structure of **Fe$_4$Ph** on gold extrapolating the molecule from the surface, *i.e.* removing the gold substrate without any further relaxation.

The evaluated *J*s reported in the third row of the left part of Table 1 show minor changes, in agreement with the small modifications observed in the molecular geometry upon adsorption. Additional electronic effects induced by the substrate are however neglected at this level of treatment.

Table 1: *J* values (in cm^{-1}) computed on experimental and optimized **Fe$_4$Ph** geometries with different approaches. U values for all atomic species except Au[a] are taken from ref.[35]

	PBE0			**revPBE+U**		
	J_1	J_2	$\Delta E_{5,4}$[b]	J_1	J_2	$\Delta E_{5,4}$[b]
Fe$_4$Ph$^{(X\text{-ray structure})}$	14.4	0.3	34	17.0	0.4	40
Fe$_4$Ph$^{(Optimized\ structure)}$	13.8	0.2	33	16.7	0.3	40
Fe$_4$Ph@Au $^{(Extrapolated)}$	14.7	0.1	36	17.9	0.2	43
Fe$_4$Ph@Au[a]	-	-	-	15.0÷18.8	0.31÷-1.2	35÷56
Experimental	16.37(12)	0.29(11)	42			

[a] Computed adding a U_{Au5d} value which varies from 0 to 0.6 eV. The chosen range is the one compatible with the Au(111) UPS spectrum. The corresponding ranges of computed J_1, J_2, $\Delta E_{5,4}$ values are reported (see SI for more details).[b] Energy gap between the ground $S = 5$ and the two first-excited $S = 4$ states.

In order to investigate the whole molecule-plus-substrate system (**Fe$_4$Ph@Au**), without losing the accuracy achievable with hybrid functional, we employed a less demanding approach, based on an alternative parametric method, DFT+U.[36,37] In this framework a HF-like potential (U)

describing the interaction between electrons localized on the same center (on-site interactions) was introduced. The choice of the U parameters is critical for a correct description of the electronic structure, and the values employed here were previously optimized by reproducing both the magnetic properties of the isolated molecule, right part of Table 1, and the experimental valence band structure of **Fe$_4$Ph** obtained by Ultraviolet Photoelectron Spectroscopy (UPS).[35] A range of values for U_{Au5d} was employed ~~given the incertitude on its choice~~ and the resulting exchange constants for **Fe$_4$Ph@Au** varied consequently. The overall scenario of a dominant antiferromagnetic J_1 interaction is however preserved, with a ground state S = 5 separated by 35÷56 cm^{-1} from the excited S = 4 states. A slight increase of the $\Delta E_{5,4}$ is observed when larger U_{Au5d} values are considered. The results of this investigation indicate only minor effects induced by the interaction of **Fe$_4$Ph** with the substrate. The magnetic anisotropy, not included in our treatment, is also expected to be substantially unaffected due to the minor geometrical modifications and almost negligible electronic effects arising from the proximity of the metallic substrate.

Experimental insight into the electronic structure and magnetic behavior of a surface-supported **Fe$_4$Ph** submonolayer was obtained through synchrotron-based X-ray absorption techniques, a key tool for the investigation of thin deposits of magnetic molecules.[38,39] Surface selectivity and sensitivity to submonolayer coverages is in fact achieved by measuring the absorption in the Total Electron Yield (TEY) mode,[40] which is based on the emission of secondary electrons and the detection of the current flow to re-establish neutrality. Moreover, X-ray absorption based experiments involve core orbitals and are element and oxidation-state selective. Finally, by employing circularly polarized light with opposite helicities and measuring the absorption with

right (σ^-) and left (σ^+) polarized light (see SI), X-ray Magnetic Circular Dichroism (XMCD) is evaluated as $\sigma^- - \sigma^+$, thus obtaining information on the magnetic moment at the probed atoms.

A submonolayer of **Fe$_4$Ph**, *ca.* 0.5 ML, thus intermediate between the two coverages studied by STM, was sublimated *in-situ* and investigated using synchrotron radiation (see SI). The XAS spectra recorded at the Fe $L_{2,3}$ edge ~~on a submonolayer of **Fe$_4$Ph** on Au~~ (Fig.1c) are typical for this class of propeller-like complexes[41] suggesting that the contaminant domains are mainly formed by metal-free organic fragments. The amplitude and shape of the XMCD signal, with a vanishing response in between the two main peaks of the L_3 edge (707.9 eV), are also similar to those found in other derivatives,[41] either as bulk phases or chemisorbed on gold. They have been associated to the ferrimagnetic spin arrangement in the ground $S = 5$ state and are therefore diagnostic of intact **Fe$_4$Ph** molecules.[19,42,43]

The ^{3}He-^{4}He dilution cryostat[44] available at the beamline allowed to reach sub-kelvin temperatures and to record magnetic hysteresis curves by monitoring the field dependence of the XMCD signal at the energy of its maximum amplitude (709.1 eV). The results obtained at three different temperatures are reported in Fig. 4. The measurement at the lowest accessible temperature (0.68 K) was carried out at two different orientations of the magnetic field with respect to the surface normal, *i.e.* $\theta = 0°$ and 45° (see inset of Fig.1c for a scheme of the experiment). The temperature dependence is in line with previous measurements on bulk as well as chemisorbed SMMs of the same family.[42,43] A butterfly shaped hysteresis loop is recovered at this temperature with well-defined steps around zero field and ±5 kOe. An important feature is that the observed step positions for $\theta = 0°$ are in good agreement with those expected for resonant quantum tunneling of the magnetization (QTM)[3] when the magnetic field is applied along the easy axis (z), *i.e.* $H = 0$ and $H = \pm|D|/(g\mu_B) = 4.5$ kOe. Furthermore, the steps shift to

higher field on increasing the θ angle. Finally, the XMCD signal at θ = 0° levels off at low field, while a more gradual increase at higher fields is observed for θ = 45°. A similar behavior was previously found in a monolayer of a sulfur-functionalized Fe_4 derivative[24] and attributed to a preferential grafting of the molecules with their easy axis perpendicularly to the surface. Such a partial ordering of **Fe_4Ph** molecules is in line with our *ab initio* calculations presented above.

We also directly probed the time dependence of the magnetization at 0.68 K by first magnetizing the system in a +16 kOe magnetic field, fast sweeping the field to -2.5 kOe and then monitoring the time evolution of the XMCD signal at 709.1 eV. This particular field was chosen as it lies in between the resonant QTM steps and consequently affords the slowest magnetic relaxation. Notice that in zero-field the magnetization dynamics is too fast to be measured by XMCD and, additionally, the signal/noise response of the TEY detector becomes much worse. The investigation has been carried out at both θ angles and the characteristic time of the decay, *i.e.* 1400 ± 100 s and 1100 ± 100 s for θ = 0° and θ = 45°, respectively, has been evaluated by fitting the experimental data to a mono-exponential law.

Following a previously developed approach, we used quantum master matrix[24] calculations to reproduce the temperature and angular dependence of the hysteresis curves reported in Fig. 4. This numerical approach allows to take into account a preferential orientation of the molecules on the surfaces. It has recently been shown that propeller-like SMMs have non-zero sixth-order transverse terms, very efficient in promoting QTM at low temperature, as a result of the multispin nature and the non-collinearity of the anisotropy tensors.[45] Even if a best-fit procedure was not feasible an acceptable agreement was obtained with D/k_B = -0.6 K, E/k_B = 0.02 K, B_4^3/k_B = 0.005 K and B_6^6/k_B = 3×10^{-6} K, where E embodies the second-order rhombic anisotropy, and the last two terms describe fourth and sixth-order transverse anisotropies that are

relevant in Fe_4 complexes.[3,45,46] The inclusion of a sixth-order term allowed to significantly reduce the other transverse terms, compared to values previously employed to simulate the hysteresis of a self-assembled monolayer, though they are still larger than those observed for similar derivatives in the crystalline phase.[45] Moreover the easy magnetic axes were restricted to be randomly distributed within the angular range 30° - 40° from the surface normal, without any preferential in-plane orientation, as suggested by DFT calculations. An additional contribution of 20% randomly-oriented molecules was introduced as the magnetization does not achieve full saturation. No evidence of fast relaxing species emerged from the simulation of the hysteresis.

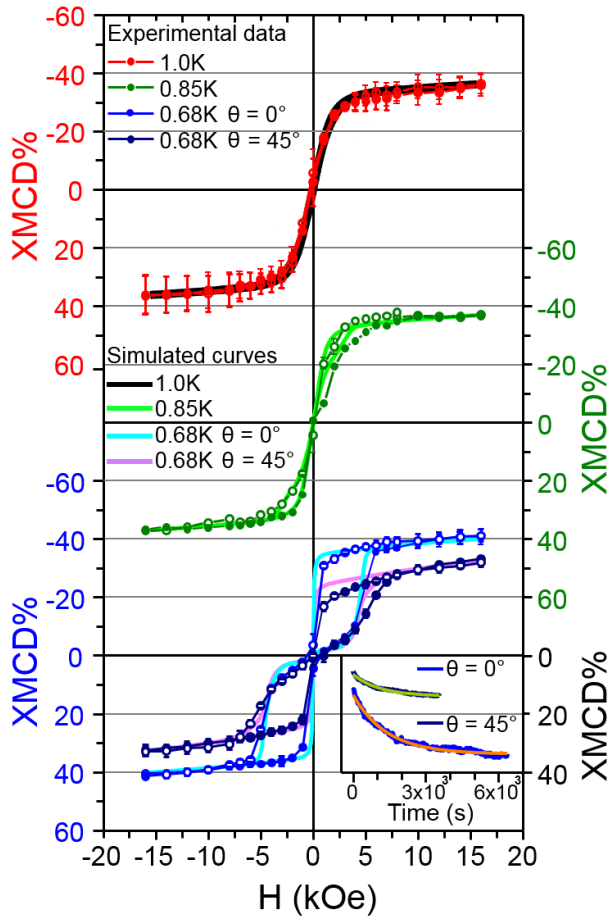

Figure 4. Temperature-dependent hysteresis loops acquired by monitoring the field dependence of the XMCD signal at 709.1 eV; at the lowest temperature the hysteresis loop has been

measured at θ = 0° (blue) and θ = 45° (dark blue). Data recorded with decreasing field are indicated as empty symbols. Each experimental hysteresis loop is superimposed to the calculated one. The acquisition of a full hysteresis loop required *ca.* 90 min. The inset presents time decay data recorded at -2.5 kOe after saturation at +16 kOe; the solid lines are fits to a mono-exponential law (green θ = 45° and orange θ = 0°); data are expressed in the same reference scale as the hysteresis loops.

Though the strong correlation between parameters prevented the determination of a unique set of spin Hamiltonian parameters, the good agreement with experimental data at this level of approximation further confirms that **Fe$_4$Ph** is able to retain its SMM properties at the submonolayer level. It is interesting to notice that magnetization jumps at resonant fields (H = 0 and ±5 kOe) occur in a narrower field range in calculated hysteresis loops than in the experimental ones. This discrepancy could arise from neglecting local dipolar fields in our simulation. In a three-dimensional (3D) crystal of magnetically-saturated molecules, the magnitude and orientation of local dipolar fields are crucially dependent on the crystal structure. By contrast, in a bidimensional (2D) lattice of molecules magnetized perpendicular to the surface (say, along –Z), the local dipolar fields are always oriented antiparallel to the magnetizing field (*i.e.* along +Z). Furthermore, since dipolar contributions from all sites sum up constructively, dipolar fields can easily exceed those typical of 3D arrays. Sample calculations assuming a hexagonal 2D lattice with 1.6 nm spacing between S=5 spins reveal a dipolar bias of *ca.* 24 mT, hence significantly larger than for a related 3D crystal.[47] Peculiar is also the evolution of local dipolar fields during magnetic relaxation ("dipolar shuffling").[48] After the system is initialized with all magnetic moments along –Z (lower left branch of the hysteresis loop in Fig. 4), spin reversal is expected to start at a slightly negative H value due to the positive dipolar bias.

Because reversing some spins diminishes the dipolar bias on the array, the remaining spins will have additional possibilities to flip at higher *H* values, *i.e.* later in the sweep. Though a quantitative analysis is beyond the scope of this work, such "dipolar shuffling" effects are predicted to broaden magnetization steps and, in addition, to favor relaxation. The evolution of dipolar fields can indeed explain why oriented 2D arrays of SMMs display no remnant magnetization and a more pronounced tunneling, thus justifying why larger transverse anisotropy terms are necessary to simulate their hysteresis loop. We anticipate here that a more pronounced bistability may result for isolated SMMs on a surface as compared with a densely-packed monolayer.

In summary, through a combined morphological and spectroscopic characterization we demonstrated here that **Fe_4Ph** SMMs can be sublimated on gold with layer-by-layer growth of partially-oriented molecules. More importantly, we showed that at submonolayer coverage the magnetic bistability of the magnetization is preserved after this UHV-based deposition approach with enhanced tunneling due to the bidimensional arrangement of the SMMs. These findings suggest a weak interaction with the gold substrate that was confirmed by state-of-the-art first principles calculations.

Even though a detailed *in-situ* characterization has evidenced the unavoidable co-presence of contaminants, such deposition conditions are suitable to address intact and isolated molecules by STM methods. Furthermore, they open the perspective of assembling in UHV conditions molecular-inorganic hybrid architectures that can be useful in spintronic devices.

ASSOCIATED CONTENT

XPS calibration of molecular film thickness, series of STM supporting images; information on the XAS and XMCD experimental procedures; computation details. This material is available free of charge via the Internet at http://pubs.acs.org

AUTHOR INFORMATION

Corresponding Author

* (R.S.) roberta.sessoli@unifi.it

Author Contributions

The manuscript was written through contributions of all authors.

ACKNOWLEDGMENT

We acknowledge the financial contribution of the European Research Council through the Advanced GrantMolNanoMaS (267746), of Italian MIUR through FIRB project RBAP117RWN, and of CINECA trough the ISCRA initiative. The support of the EC through the FP7/2007-2013 Calypso project (nº 31228) and of Ente Cassa di Risparmio di Firenze is also acknowledged.

We thank L. Joly, J.-P. Kappler, B. Muller, and F. Scheurer for their contribution in installing the IMPMC-IPCMS-SOLEIL dilution refrigerator. We acknowledge SIM staff for the beamline management. We also thank the CINECA award under the ISCRA initiative, for the availability of high performance computing resources and support.

REFERENCES

(1) Thomas, L.; Lionti, F.; Ballou, R.; Gatteschi, D.; Sessoli, R.; Barbara, B. *Nature* **1996**, *383*, 145–147.

(2) Friedman, J.; Sarachik, M.; Tejada, J.; Ziolo, R. *Phys. Rev. Lett.* **1996**, *76*, 3830–3833.

(3) Gatteschi, D.; Sessoli, R.; Villain, J. *Molecular Nanomagnets*; Oxford University Press, Ed.; Oxford, 2006.

(4) Bogani, L.; Wernsdorfer, W. *Nat. Mater.* **2008**, *7*, 179–186.

(5) Komeda, T.; Isshiki, H.; Liu, J.; Zhang, Y.-F.; Lorente, N.; Katoh, K.; Breedlove, B. K.; Yamashita, M. *Nat. Commun.* **2011**, *2*, 217.

(6) Schwöbel, J.; Fu, Y.; Brede, J.; Dilullo, A.; Hoffmann, G.; Klyatskaya, S.; Ruben, M.; Wiesendanger, R. *Nat. Commun.* **2012**, *3*, 953.

(7) Fu, Y.-S.; Schwöbel, J.; Hla, S.-W.; Dilullo, A.; Hoffmann, G.; Klyatskaya, S.; Ruben, M.; Wiesendanger, R. *Nano Lett.* **2012**, *12*, 3931–3935.

(8) Jo, M.-H.; Grose, J. E.; Baheti, K.; Deshmukh, M. M.; Sokol, J. J.; Rumberger, E. M.; Hendrickson, D. N.; Long, J. R.; Park, H.; Ralph, D. C. *Nano Lett.* **2006**, *6*, 2014–2020.

(9) Burzurí, E.; Yamamoto, Y.; Warnock, M.; Zhong, X.; Park, K.; Cornia, A.; van der Zant, H. S. J. *Nano Lett.* **2014**, *14*, 3191-3196..

(10) Barraza-Lopez, S.; Park, K.; García-Suárez, V.; Ferrer, J. *Phys. Rev. Lett.* **2009**, *102*, 246801.

(11) Urdampilleta, M.; Klyatskaya, S.; Cleuziou, J.-P.; Ruben, M.; Wernsdorfer, W. *Nat. Mater.* **2011**, *10*, 502–506.

(12) Vincent, R.; Klyatskaya, S.; Ruben, M.; Wernsdorfer, W.; Balestro, F. *Nature* **2012**, *488*, 357–360.

(13) Zyazin, A. S.; van den Berg, J. W. G.; Osorio, E. A.; van der Zant, H. S. J.; Konstantinidis, N. P.; Leijnse, M.; Wegewijs, M. R.; May, F.; Hofstetter, W.; Danieli, C.; Cornia, A. *Nano Lett.* **2010**, *10*, 3307–3311.

(14) Ishikawa, N.; Sugita, M.; Tanaka, N.; Ishikawa, T.; Koshihara, S.; Kaizu, Y. *Inorg. Chem.* **2004**, *43*, 5498–5500.

(15) Gonidec, M.; Biagi, R.; Corradini, V.; Moro, F.; De Renzi, V.; del Pennino, U.; Summa, D.; Muccioli, L.; Zannoni, C.; Amabilino, D. B.; Veciana, J. *J. Am. Chem. Soc.* **2011**, *133*, 6603–6612.

(16) Klar, D.; Candini, A.; Joly, L.; Klyatskaya, S.; Krumme, B.; Ohresser, P.; Kappler, J.-P.; Ruben, M.; Wende, H. *Dalton Trans.* **2014**, *43*, 10686–10689.

(17) Mannini, M.; Bertani, F.; Tudisco, C.; Malavolti, L.; Poggini, L.; Misztal, K.; Menozzi, D.; Motta, A.; Otero, E.; Ohresser, P.; Sainctavit, Ph.; Condorelli, G. G.; Dalcanale, E.; Sessoli, R. *Nat. Commun.* **2014**, *5*, 4582.

(18) Stepanow, S.; Honolka, J.; Gambardella, P.; Vitali, L.; Abdurakhmanova, N.; Tseng, T.-C.; Rauschenbach, S.; Tait, S. L.; Sessi, V.; Klyatskaya, S.; Ruben, M.; Kern, K. *J. Am. Chem. Soc.* **2010**, *132*, 11900–11901.

(19) Margheriti, L.; Chiappe, D.; Mannini, M.; Car, P.-E.; Sainctavit, Ph.; Arrio, M.-A.; de Mongeot, F. B.; Cezar, J. C.; Piras, F. M.; Magnani, A.; Otero, E.; Caneschi, A.; Sessoli, R. *Adv. Mater.* **2010**, *22*, 5488–5493.

(20) Lodi Rizzini, A.; Krull, C.; Balashov, T.; Kavich, J. J.; Mugarza, A.; Miedema, P. S.; Thakur, P. K.; Sessi, V.; Klyatskaya, S.; Ruben, M.; Stepanow, S.; Gambardella, P. *Phys. Rev. Lett.* **2011**, *107*, 177205.

(21) Lodi Rizzini, A.; Krull, C.; Balashov, T.; Mugarza, A.; Nistor, C.; Yakhou, F.; Sessi, V.; Klyatskaya, S.; Ruben, M.; Stepanow, S.; Gambardella, P. *Nano Lett.* **2012**, *12*, 5703–5707.

(22) Malavolti, L.; Poggini, L.; Margheriti, L.; Chiappe, D.; Graziosi, P.; Cortigiani, B.; Lanzilotto, V.; de Mongeot, F. B.; Ohresser, P.; Otero, E.; Choueikani, F.; Sainctavit, Ph.; Bergenti, I.; Dediu, V. A.; Mannini, M.; Sessoli, R. *Chem. Commun.* **2013**, *49*, 11506–11508.

(23) Mannini, M.; Pineider, F.; Sainctavit, Ph.; Danieli, C.; Otero, E.; Sciancalepore, C.; Talarico, A. M.; Arrio, M.-A.; Cornia, A.; Gatteschi, D.; Sessoli, R. *Nat. Mater.* **2009**, *8*, 194–197.

(24) Mannini, M.; Pineider, F.; Danieli, C.; Totti, F.; Sorace, L.; Sainctavit, Ph.; Arrio, M.-A.; Otero, E.; Joly, L.; Cezar, J. C.; Cornia, A.; Sessoli, R. *Nature* **2010**, *468*, 417–421.

(25) Margheriti, L.; Mannini, M.; Sorace, L.; Gorini, L.; Gatteschi, D.; Caneschi, A.; Chiappe, D.; Moroni, R.; de Mongeot, F. B.; Cornia, A.; Piras, F. M.; Magnani, A.; Sessoli, R. *Small* **2009**, *5*, 1460–1466.

(26) Rigamonti, L.; Piccioli, M.; Malavolti, L.; Poggini, L.; Mannini, M.; Totti, F.; Cortigiani, B.; Magnani, A.; Sessoli, R.; Cornia, A. *Inorg. Chem.* **2013**, *52*, 5897–5905.

(27) The dimension has been estimated as the largest intramolecular distance, corresponding to a pair of H atoms of the *dpm* ligands, increased by the corresponding Van der Waals radii.

(28) Zhang, Y.; Yang, W. *Phys. Rev. Lett.* **1998**, *80*, 890.

(29) Grimme, S.; Antony, J.; Ehrlich, S.; Krieg, H. *J. Chem. Phys.* **2010**, *132*, 154104.

(30) Noodleman, L.; Norman, J. G. *J. Chem. Phys.* **1979**, *70*, 4903.

(31) Noodleman, L. *J. Chem. Phys.* **1981**, *74*, 5737.

(32) Totti, F.; Rajaraman, G.; Iannuzzi, M.; Sessoli, R. *J. Phys. Chem. C* **2013**, *117*, 7186–7190.

(33) Adamo, C.; Barone, V.; Bencini, A.; Totti, F.; Ciofini, I. *Inorg. Chem.* **1999**, *38*, 1996–2004.

(34) Adamo, C.; Barone, V. *J. Chem. Phys.* **1999**, *110*, 6158.

(35) Ninova, S.; Lanzilotto, V.; Malavolti, L.; Rigamonti, L.; Cortigiani, B.; Mannini, M.; Totti, F.; Sessoli, R. *J. Mater. Chem. C* **2014**, in press. doi:10.1039/C4TC01647E.

(36) Anisimov, V. I.; Zaanen, J.; Andersen, O. K. *Phys. Rev. B* **1991**, *44*, 943–954.

(37) Cococcioni, M.; de Gironcoli, S. *Phys. Rev. B* **2005**, *71*, 035105.

(38) Cornia, A.; Mannini, M. Structure and Bonding; Springer Berlin Heidelberg, 2014; pp. 1–38.

(39) Sessoli, R.; Mannini, M.; Pineider, F.; Cornia, A.; Sainctavit, P. In *Magnetism and synchrotron radiation*; Springer, Ed.; Berlin, 2010; pp. 279–311.

(40) Nakajima, R.; Stöhr, J.; Idzerda, Y. U. *Phys. Rev. B* **1999**, *59*, 6421–6429.

(41) Mannini, M.; Pineider, F.; Sainctavit, Ph.; Joly, L.; Fraile-Rodríguez, A.; Arrio, M.-A.; Cartier dit Moulin, C.; Wernsdorfer, W.; Cornia, A.; Gatteschi, D.; Sessoli, R. *Adv. Mater.* **2009**, *21*, 167–171.

(42) Accorsi, S.; Barra, A.-L.; Caneschi, A.; Chastanet, G.; Cornia, A.; Fabretti, A. C.; Gatteschi, D.; Mortalo, C.; Olivieri, E.; Parenti, F.; Rosa, P.; Sessoli, R.; Sorace, L.; Wernsdorfer, W.; Zobbi, L. *J. Am. Chem. Soc.* **2006**, *128*, 4742–4755.

(43) Cornia, A.; Fabretti, A. C.; Garrisi, P.; Mortalò, C.; Bonacchi, D.; Gatteschi, D.; Sessoli, R.; Sorace, L.; Wernsdorfer, W.; Barra, A.-L. *Angew. Chem. Int. Ed. Engl.* **2004**, *43*, 1136–1139.

(44) Letard, I.; Sainctavit, Ph.; dit Moulin, C. C.; Kappler, J.-P.; Ghigna, P.; Gatteschi, D.; Doddi, B. *J. Appl. Phys.* **2007**, *101*, 113920.

(45) Sorace, L.; Boulon, M.-E.; Totaro, P.; Cornia, A.; Fernandes-Soares, J.; Sessoli, R. *Phys. Rev. B* **2013**, *88*, 104407.

(46) Abragam, A.; Bleaney, B. *Electron Paramagnetic Resonance of Transition Ions*; S, Ed.; Dover: New York, 1986.

(47) Vergnani, L.; Barra, A.-L.; Neugebauer, P.; Rodriguez-Douton, M. J.; Sessoli, R.; Sorace, L.; Wernsdorfer, W.; Cornia, A. *Chemistry* **2012**, *18*, 3390–3398.

(48) Liu, J.; Wu, B.; Fu, L.; Diener, R.; Niu, Q. *Phys. Rev. B* **2002**, *65*, 224401.

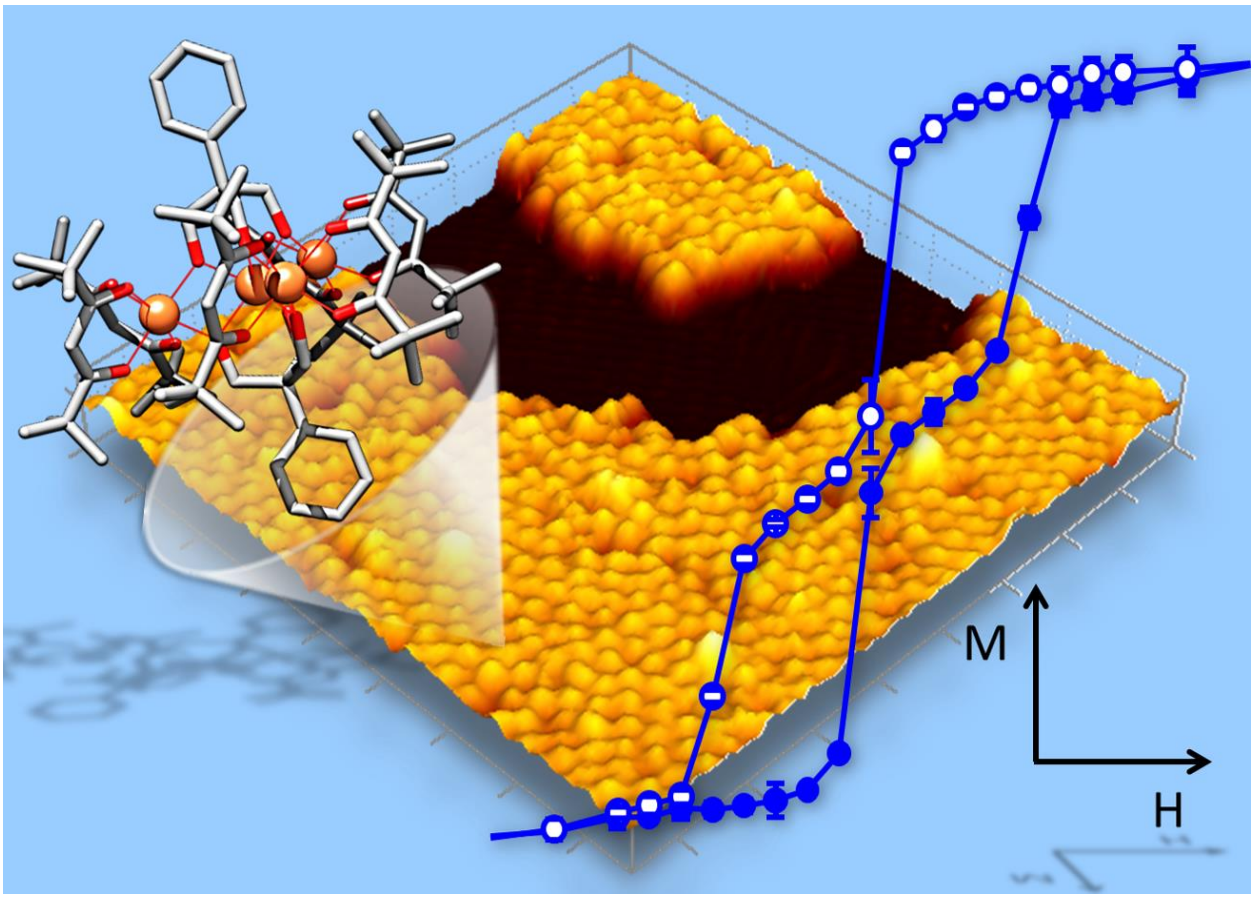
M
H